

Friction damping and forced-response of vibrating structures: an insight into model validation

*Original*

Friction damping and forced-response of vibrating structures: an insight into model validation / Umer, Muhammad; Gastaldi, Chiara; Botto, Daniele. - In: INTERNATIONAL JOURNAL OF SOLIDS AND STRUCTURES. - ISSN 0020-7683. - ELETTRONICO. - 202:(2020), pp. 521-531. [10.1016/j.ijsolstr.2020.07.002]

*Availability:*

This version is available at: 11583/2841296 since: 2020-07-24T09:25:46Z

*Publisher:*

Elsevier

*Published*

DOI:10.1016/j.ijsolstr.2020.07.002

*Terms of use:*

This article is made available under terms and conditions as specified in the corresponding bibliographic description in the repository

*Publisher copyright*

Elsevier postprint/Author's Accepted Manuscript

© 2020. This manuscript version is made available under the CC-BY-NC-ND 4.0 license  
<http://creativecommons.org/licenses/by-nc-nd/4.0/>. The final authenticated version is available online at:  
<http://dx.doi.org/10.1016/j.ijsolstr.2020.07.002>

(Article begins on next page)

# Friction damping and forced-response of vibrating structures: an insight into model validation

Muhammad Umer<sup>a</sup>, Chiara Gastaldi<sup>b</sup>, Daniele Botto<sup>b,\*</sup>

<sup>a</sup>*Mechanical Engineering Department - Institute of Space Technology, Islamabad, Pakistan*

<sup>b</sup>*Department of Mechanical and Aerospace Engineering - Politecnico di Torino, 10129 Torino, Italy*

---

## Abstract

Dry friction is widely incorporated in turbomachinery, in the form of under-platform dampers, to limit vibrations at resonance and reduce risks of high-cycle fatigue failures. Most of the test rigs that were used to investigate the behavior of under-platform dampers aim at evaluating the damper performance in terms of reduction of forced-response amplitude in blades. This approach could be insufficient to understand local nonlinearities in the contact and the influence of dampers on blade dynamics. A recently developed test rig provides the authors with an unprecedented set of information. It is capable to measure contact forces and relative displacements between dampers and blade in addition to the overall blade dynamic response. This controlled environment, together with an effective model of the blade/dampers system, is used to provide an insight into the subject of model validation. The presented experimental and numerical study of the damper is used to highlight

---

\*Corresponding author

*Email addresses:* `muhammad.umer@ist.edu.pk` (Muhammad Umer), `chiara.gastaldi@polito.it` (Chiara Gastaldi), `daniele.botto@polito.it` (Daniele Botto)

the relevance of an accurate representation of the constraints induced by friction contacts and to discuss the adequacy of state-of-the-art contact models.

*Keywords:*

Turbine blade vibrations Nonlinear dynamics Friction damping

Under-platform damper Test rig Contact force measurement

---

## 1. Introduction

Dry friction damping is used, in the field of turbomachinery, to mitigate the structural vibrations caused by fluctuating stresses [1, 2]. Under-platform dampers (UPDs) are small metallic components placed between two consecutive blades of a turbine to minimize the blade vibration by dissipating the energy exploiting friction at the contact interface. Highly nonlinear behavior of the frictional contacts makes it challenging for researchers and engineers to precisely model and predict the response of complete blade/damper system. In this regard, explicit numerical models of UPDs were used with a multi-harmonic balance [3] solver to predict their nonlinear behavior. In [4], the harmonic balance method was used with the continuation technique to compute the nonlinear modes of the damper-blade system for a large range of energy levels. Detailed studies on the modeling of UPDs were presented by several authors [5–13]. In these studies a suitable contact model was adopted to compute the damper contact forces as a function of given relative displacement between two contact surfaces. Contact models must be calibrated and validated using experimental results. This step is crucial as numerical results are strongly dependent on the chosen set of contact parameters namely friction coefficient and contact stiffness, [12, 14–16]. Therefore, experimental

20 measurements are necessary:

- to determine the performance of the damper in terms of blade amplitude reduction and frequency shift;
- to estimate the contact parameters used to calibrate contact models.

These two necessities are sometimes fulfilled with the same set of experimental evidence usually in the form of Frequency Response Functions (FRFs) [9, 17–19]. Unfortunately, model updating based on contact parameters to obtain the desired frequency response is not a viable practice, as multiple combinations of these parameters may produce the same frequency response resulting in an under-determined problem. Another way to obtain contact parameters is through the use of single-contact test arrangements[20–22]. An improved test rig [23] was capable of measuring friction coefficients and contact stiffness of a flat-on-flat contact interface. This test rig had the facility to control the relative displacement of the contacting surfaces and to operate at high temperature. However, the constant normal load applied to the contact surface was not consistent with the real operating conditions of UPDs in which the normal load varies during a cycle. An upgrade first proposed in 2010 [24] had a single damper constrained between two dummy platforms. A feedback controlled displacement was provided with the help of piezoelectric actuator on one of the platform whereas, damper contact forces were measured on the other platform by using two load cells. This test rig was used to investigate the kinematics of several dampers [25, 26]. Experimental results obtained with this rig were also used to validate a contact model based on a modified Iwans model [27], an alternative method instead

of solving the specific contact problem as proposed in [28]. In this test rig the  
45 blade platform kinematics was imposed by the experimenter, thus the effect  
of the damper on the blade dynamics was not present. Therefore, a novel  
test bench [29, 30] was designed by the authors to overcome these limitations  
and investigate the relationship between the damper kinematics and blade  
dynamics (a topic of recent interest in the engineering community [12]). This  
50 experimental setup was composed of a single turbine blade with two UPDs  
and had the capability to measure the damper contact forces, its relative  
displacement with respect to the blade and the blade response.

Data obtained with this experimental setup establish a base to study the  
55 behavior of dampers at their contact level. Moreover, the measured contact  
forces offer the unprecedented opportunity to validate directly the Finite El-  
ement (FE) model of the blade subjected to nonlinear contact forces. In  
fact, measured contact forces can be applied as external forces on the FE  
model of the blade. The resulting numerical FRF can then be compared to  
60 its experimental counterpart. Results of this comparison show that given  
combinations of blade mode shape and platform angles lead to very small  
contact forces, close to the accuracy of the measuring device. Uncertainty in  
the amplitude and phase of the contact forces could prevent the test rig from  
gathering meaningful evidence from the contact forces signal. Furthermore,  
65 very small contact forces can lead to a negligible effect of the damper on the  
blade dynamics. The purpose of the work presented in this paper is to de-  
velop a procedure to evaluate the sensitivity of the contact forces to different  
platform angles. To this end, the idea of implicit stiffness was introduced.

The authors believe that the proposed approach will provide guidance in the  
70 design of any laboratory set-up and in the estimation the UPD potential in  
realistic operating conditions.

This paper is organized as follows: Sect. 2 gives a brief description of the  
test rig used in the experimental campaign; Sect. 3 addresses the numeri-  
75 cal model of the blade while Sect. 4 shows the procedure used to validate  
the dynamic model in which the contact forces between under-platform and  
damper are replaced by their measured counterparts; Sect. 5 presents and  
validates a numerical tool that, for a given blade model, maps the contact  
forces as a function of the platform angles; Sect. 6 summarizes the results  
80 and the main achievements of the paper.

## 2. Experimental Setup

The feature that best distinguishes the present test rig from others found  
in the literature is the measurement of the contact forces when the damper  
is dynamically coupled with the blade. A top view of the test rig is shown in  
85 Fig.1 which presents a single turbine blade and two dampers. The dampers  
are in contact with the under-platform of the blade on one side and with  
a ground platform on the other side. Each ground platform, one for each  
damper, is linked to a contact force measuring system. The two ground plat-  
form are referred to as “Even” or “Odd” after the serial number of the load  
90 cells installed on that platform. A component named L-Separator, designed  
with two orthogonal limbs, separates the contact forces into two components  
acting along each limb axes. A piezoelectric load cell is placed at the end

of each limb to measure the respective force component. Each load cell undergoes an axial force while the tangential component is negligible. This  
95 condition was achieved by designing the limbs of the L-Separator with a very high ratio between the longitudinal and transverse stiffness. With this design the side effects related to friction and sliding at the interfaces between the load cell and the limb or the ground are minimized. The cross-talk effect is avoided as well. The lowest in-plane natural frequency of the force measuring  
100 system, L-Separator with load cells and coupling devices, is about 4380 Hz. Therefore the rig can operate at high excitation frequencies, up to 4 kHz, without triggering resonances. A controllable and measurable pushing force  $F_P$  is applied on the root of the blade - to simulate the actual centrifugal force which acts on the blade while the turbine runs, see also Fig. 2 - through a  
105 pushing block. In [30] an exhaustive description of the rig and of the force measuring system along with its sensitivity is reported.

The contact forces at the blade platform side are inferred from the measured contact forces at the ground platform side through a simple force equilibrium, depicted in Fig. 2. The damper inertia forces are here neglected, a  
110 perfectly valid assumption at frequencies lower than 5 kHz as demonstrated in [31]. Forces are decomposed into their normal (N) and tangential (T) components, as shown in Fig. 2, or along the blade axial-radial directions (XYZ reference system). This last reference system is the same adopted in  
115 the FE model of the blade and will be used throughout the paper. The blade excitation is provided by means of an electromagnetic shaker. The shaker stinger is connected at a point near the blade root (low mobility point) to

excite the structure at a given frequency with the desired excitation level.

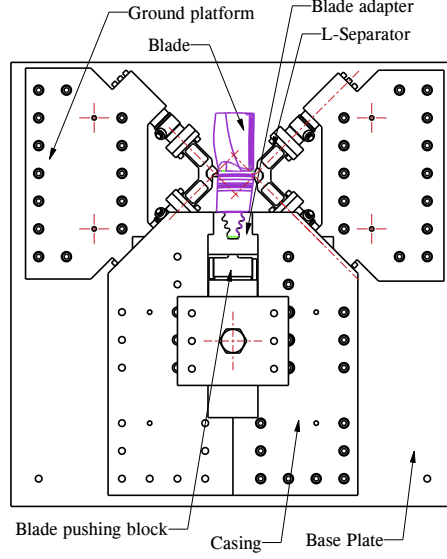


Figure 1: Top view of the test rig

### 3. The blade numerical model

The general dynamic equation of any friction-damped system can be written as

$$\mathbf{M}\ddot{\mathbf{Q}} + \mathbf{C}\dot{\mathbf{Q}} + \mathbf{K}\mathbf{Q} = \mathbf{F}_E + \mathbf{F}_C \quad (1)$$

where  $\mathbf{M}$ ,  $\mathbf{C}$  and  $\mathbf{K}$  correspond to mass, damping and stiffness matrices of the system respectively. In Eq.1, vector  $\mathbf{Q}$  represents the displacement of all degrees of freedoms (DOFs) of the system. Vectors  $\mathbf{F}_E$  and  $\mathbf{F}_C$  correspond to external and contact forces respectively. In the present case, the external force  $\mathbf{F}_E$  is applied through an electromagnetic shaker, whereas  $\mathbf{F}_C$  are non-linear forces at the blade platform-damper contact interface. The mass and



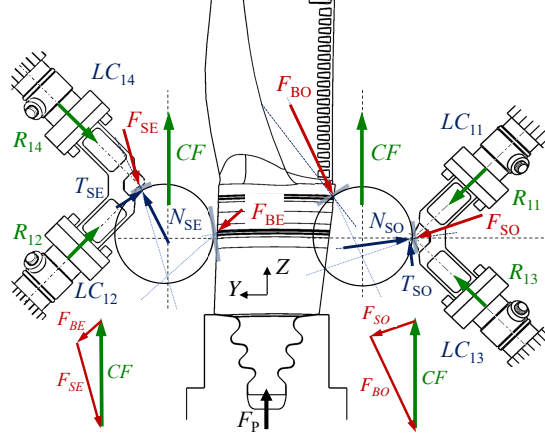


Figure 2: Damper static force equilibrium.  $R_{ij}$  are the forces read by load cells  $LC_{ij}$ . Contact forces  $F$  are resolved into normal  $N$  and tangential  $T$  components. Subscript  $S$  or  $B$  means force on Support or Blade, while  $E$  or  $O$  denotes the “Even” or the “Odd” side. Sides are named Even or Odd after the serial number of the load cells installed on that side. The static load  $CF$ , simulating the Centrifugal Force on dampers, is applied with dead weight.

stiffness matrices of the blade were obtained using a commercial FE code. The number of DOFs in a FE model is generally very high, so it could be very demanding to run dynamic analysis if non linearity due to contact problems are present. Moreover, commercial codes are not so flexible and open-source  
130 to accept external routines developed by users to solve special problems or to test new solution methods. For these reasons the mass and stiffness matrices of the full FE model were reduced and exported to be used together with in-house developed codes.

### 3.1. Craig-Bampton Model Order Reduction

135 The Craig-Bampton reduction method [32–34], also known as CB-CMS, is a commonly used technique to reduce the size of a large FE model by acquiring the fundamental frequency modes of the structure. In this method, a subset of physical DOFs of the full model are retained as master DOFs while the remaining DOFs are reduced in a set of orthogonal modes, denoted to as  
140 slave DOFs.

Figure 3 shows the blade FE model and the nodes chosen as master nodes in the CMS reduction. The contact line between the cylindrical damper and the under-platform was represented by 7 contact nodes on each blade platform. The root attachment was modeled with 95 nodes on the left side and  
145 94 nodes on the right side (the attachment is not symmetric). One excitation node was used for the blade excitation, where the shaker was attached, and acceleration node was used for blade response, where the accelerometer was positioned. It was here chosen to apply the CB-CMS technique to the free blade model. Matrices  $\mathbf{M}$  and  $\mathbf{K}$  thus become  $\mathbf{M}_{\mathbf{R}}$  and  $\mathbf{K}_{\mathbf{R},\text{free}}$ . The  
150 structure will be constrained to reproduce the clamping of the root, at a subsequent step. Section 3.3 gives further details on this matter.

### 3.2. Blade Model Updating

The FE model of the blade was updated to match the first two measured natural frequencies (see response depicted in Fig. 4) in free-free conditions,  
155 i.e. without damper and blade root constraints. The Young modulus was chosen as the updating parameter while the density was estimated by measuring the blade weight with a high precision scale and assuming a uniform distribution of the mass on the 3D model. It was found that with a Young's

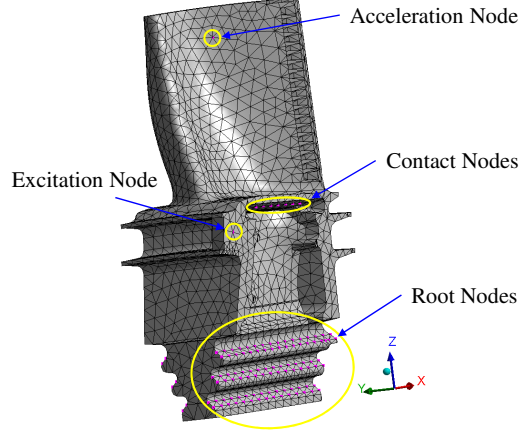


Figure 3: Finite element model of the blade and selected master nodes for CB-CMS reduction. Master nodes on one platform and one side of the root are hidden because of the orientation of the blade.

modulus of 210,000 MPa the first two resonances of the free-free blade (5652.7  
 160 and 7567.3 Hz) match well with the measured values (5652.5 and 7557.5 Hz).

### 3.3. Applying clamp boundary conditions

A very high clamping force, if compared with the excitation, was applied on the blade root. This very high force,  $F_P = 150$  kN, minimizes the relative displacement between the blade root and its slot, thus the resulting friction damping at the root is negligible. Preliminary dynamics tests were performed on the blade without dampers at different magnitudes of the excitation force  $\mathbf{F}_E$ . Results showed that the response was linearly dependent on the excitation force, proving that the friction damping (the nonlinear effect) is negligible. For this reason, the blade clamping was modeled by introducing a 3D spring element at each node on the blade roots, as shown in Fig.5. The

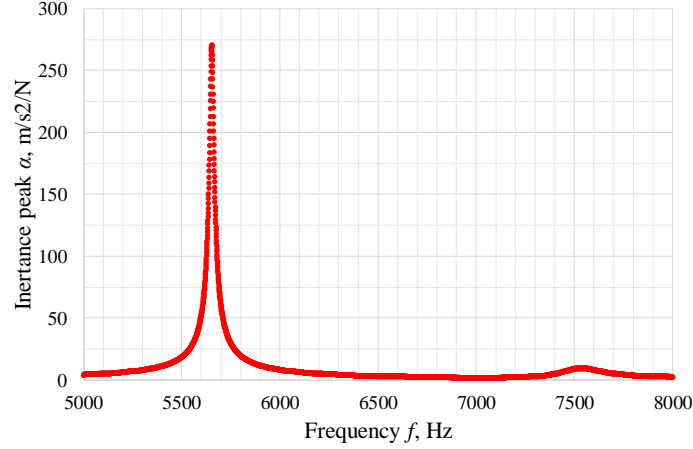


Figure 4: Measured FRFs of free-free blade.

3D spring element may connect each selected blade root node either to a corresponding node on the surrounding structure (if the disk is modeled) or simply to ground (if, as in this case, the bulkiness and stiffness of the blade adapter allows for this simplification.)

The use of a 3D spring element (which may be easily upgraded to an actual contact element capable of slip if deemed necessary) allows modeling the effect of compliance of the contact interface in all directions. The 3D spring element needs two calibration parameters:  $k_n$  and  $k_t$ , i.e. it is here assumed that the tangential stiffness in the two uncoupled directions shown in Fig. 5. share the same value  $k_{t1} = k_{t2} = k_t$ . The values of the stiffness were determined by imposing that the first two measured frequencies  $f_{meas}$  of the clamped-free (i.e. no damper) blade match the simulated ones  $f_{sim}$ ,

$$\begin{cases} f_{1,meas} = f_{1,sim}(k_n, k_t) \\ f_{2,meas} = f_{2,sim}(k_n, k_t) \end{cases} \quad (2)$$

Matrix  $\mathbf{K}_{\mathbf{R},\text{free}}$  from Sect. 3.1, is thus substituted by matrix  $\mathbf{K}_{\mathbf{R}}$ .

The damping contribution of the blade root is not accounted by the springs  
 165 (as no microslip is allowed at this stage). The (minor) contribution to damp-  
 ing given by the blade root together with the structural (material) damping  
 of the blade are included in the matrix  $\mathbf{C}_{\mathbf{R}}$ . The modal damping was esti-  
 mated using the measured FRFs of the clamped free (i.e. no damper) blade  
 as a reference. The damping ratios  $\zeta$  were found to be 0.032 and 0.022 for the  
 170 first and the second mode respectively; the resulting experimental-numerical  
 comparison is shown in Fig. 6.

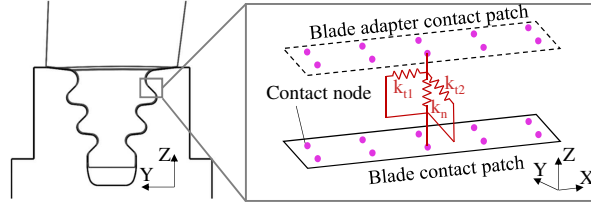
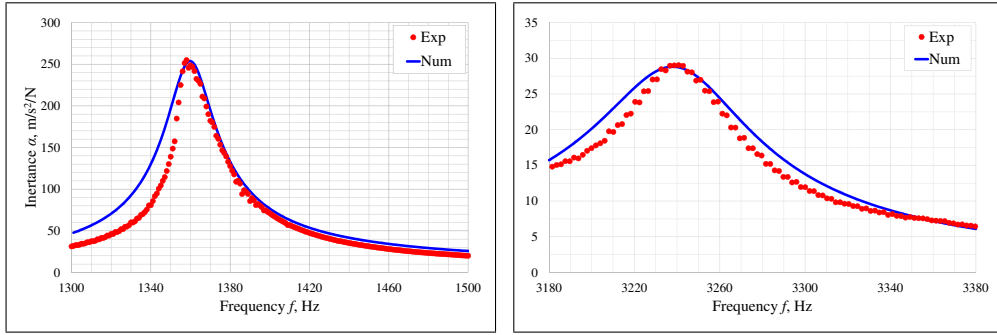


Figure 5: 3D spring compliance introduced to simulate the blade root constraints.



(a) First resonance peak

(b) Second resonance peak

Figure 6: Comparison between measured and simulated FRFs of the blade after the contact stiffness and the damping in the numerical model has been updated to an optimal value.

### 3.3.1. Forced response calculation

This section gives further details on the method used to solve the system in Eq. 1. Harmonic balance is used to compute the steady state solution of these equations where an applied periodical excitation force of frequency  $\omega$  results in the periodical response of the system [35, 36]. If the damper is not present (i.e. clamped-free blade), then  $CF = 0$ , the equilibrium is linear and can be solved, in the frequency domain, as a simple system of algebraic equations

$$\overline{\mathbf{Q}}^1 = (-\omega^2 \mathbf{M}_{\mathbf{R}} + i\omega \mathbf{C}_{\mathbf{R}} + \mathbf{K}_{\mathbf{R}})^{-1} \overline{\mathbf{F}}_{\mathbf{E}}^1 \quad (3)$$

where matrices  $\mathbf{M}$  and  $\mathbf{K}$  have been substituted with their CB-CMS reduced counterpart, later constrained at the root  $\mathbf{M}_{\mathbf{R}}$  and  $\mathbf{K}_{\mathbf{R}}$  and  $\overline{\mathbf{Q}}^1$  and  $\overline{\mathbf{F}}_{\mathbf{E}}^1$  represent the first harmonic Fourier components of the displacement and external force vectors respectively. Equation 3 can be written in a short form as

$$\overline{\mathbf{Q}}^1 = \mathbf{D}(\omega)^{-1}(\overline{\mathbf{F}}_{\mathbf{E}}^1), \quad (4)$$

whereas  $\mathbf{D}(\omega)$  corresponds to the dynamic stiffness matrix

$$\mathbf{D}(\omega) = (-\omega^2 \mathbf{M}_{\mathbf{R}} + i\omega \mathbf{C}_{\mathbf{R}} + \mathbf{K}_{\mathbf{R}}) \quad (5)$$

If, on the other hand, the damper is present, contact forces  $\mathbf{F}_{\mathbf{C}}(\mathbf{Q}, \dot{\mathbf{Q}})$  are non-zero. These forces are due to Coulomb friction nonlinearities and are typically determined as a function of relative displacements at the contact using a suitable contact model [37]. Given the dependence of contact forces on displacements, the equations are clearly nonlinear. As a result, iterative techniques such as Newton-Raphson or Continuation methods are applied [38].

In this work the theoretical contact forces were replaced by the measured contact forces. The contact force on each under-platform was uniformly distributed on the 7 contact nodes (see Fig. 3). Both measured contact forces and external forces were transformed in the frequency domain using fast Fourier transform (FFT), and applied to the clamped-free blade model so that Eq. 4 becomes

$$\bar{\mathbf{Q}}^1 = \mathbf{D}(\omega)^{-1} \left( \bar{\mathbf{F}}_{\mathbf{E},\text{meas}}^1 + \bar{\mathbf{F}}_{\mathbf{C},\text{meas}}^1 \right). \quad (6)$$

The dependence of contact forces on relative displacements is still present, in fact different experimental conditions (different  $\omega$ , different excitation levels  $|\mathbf{F}_{\mathbf{E}}|$ ) yield different measured values of  $\mathbf{F}_{\mathbf{C}}$ . However, no assumption on the formulation of this displacement-contact force relation is needed at this stage. Furthermore, this procedure is valid whichever the contact condition, including highly nonlinear states. Measured contact forces can be treated as external force vectors and, without loss of accuracy, one can obtain the first harmonic of the displacement starting from the first harmonic of the measured contact forces (as in Eq. 5). The authors are willingly separating the validation of the blade dynamic model (results in Sect. 4) from the assessment of the adequacy of the contact model formulation.

#### 4. Validation of the dynamic model blade with virtual constraints

The objective of this section is to verify if the forced response computed using the clamped FE model of the blade, fed with the measured contact forces values, is able to replicate the measured FRF. The blade response was simulated applying the procedure explained in Sect. 3. The steps of the

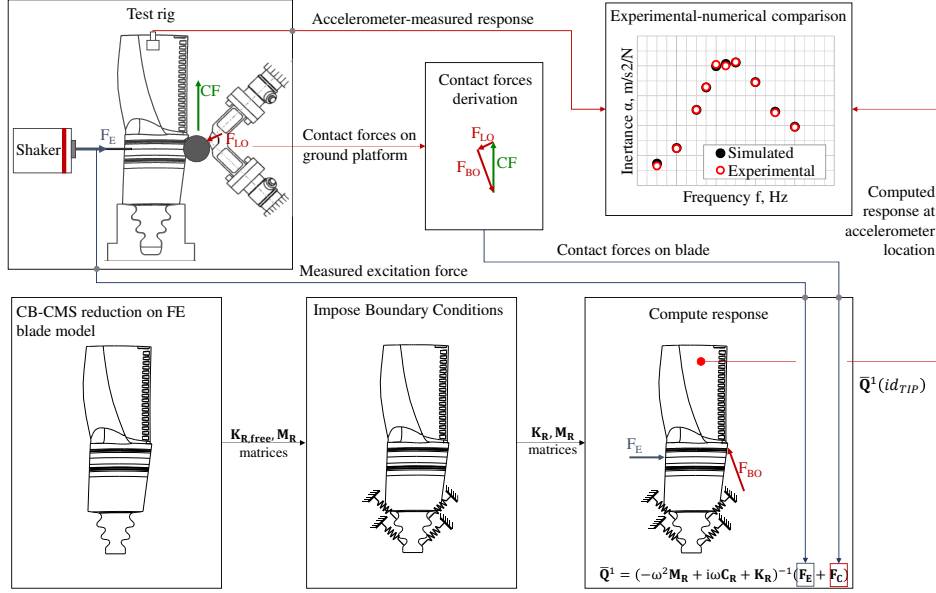


Figure 7: Algorithm describing the validation of the linear blade dynamic model

validation procedure are summarized below and displayed graphically in Fig.

190 7.

1. The blade was excited with a sinusoidal force, applied through a shaker, whose amplitude was set at  $|\mathbf{F}_E| = 1$  N in all studied cases.
2. Contact forces were measured at the ground platforms side of both dampers, whereas force components applied on the blade were inferred through the damper static force equilibrium (Fig. 2).
3. Response of the blade, in terms of inertance, was recorded by an accelerometer located at the tip of the blade.
4. The full FE model of the blade was reduced with the CB-CMS method, see Sect. 3.1, yielding a set of stiffness and mass matrices  $\mathbf{K}_{R,free}$  and  $\mathbf{M}_R$ .

200



5. A set of contact springs was applied to the root contacts as described in Sect. 3.3. The reduced order stiffness matrix  $\mathbf{K}_{\mathbf{R},\text{free}}$  thus becomes  $\mathbf{K}_{\mathbf{R}}$ .
6. The first harmonic of both the excitation and contact forces were mimicked in the numerical environment according to Eq. 6.
7. Experimental and simulated inertance were compared.

The uncertainty level of contact force measurements is in the  $[0.50 \div 0.75]$  N range, and cannot be reduced further due to mechanical tolerances, electronics, signal/noise ratio and uncertainty involved in the estimation of platform angles. Details on contact forces calculation and quantification of their uncertainty can be found in [30]. It will be shown that, depending on the magnitude of harmonic variation of the contact forces, the uncertainty level of the forces may hinder the validation procedure.

#### *4.1. Noise effect on measured contact forces*

As a first trial, both dampers were assembled at their nominal position with respect to the blade as shown in Fig. 2. A number of experiments were performed, under the same nominal experimental conditions, to measure the contact forces on both sides and the blade response. Figure 8 shows two examples of simulated responses compared with their measured counterparts. A slight variability can be detected in the measured responses despite the same nominal conditions of the test. This variability is not surprising as the dampers contact conditions may be different even if the external loads on blade and dampers are nominally the same [29, 30]. More concerning, is the poor repeatability (only two examples are reported but this effect is

present in all tests performed) and the huge discrepancy with respect to the measured response which would make the proposed method completely unreliable. The examples in Fig. 8 confirm that there is a significant discrepancy between numerical and experimental results. Furthermore, if the uncertainty on the contact force reading is taken into account and propagated through Eq. 6, a large scattering of numerical response amplitudes is obtained. This scattering is graphically represented through the error bars in Fig. 8. It is evident that this result pushes the authors further to thoroughly review the proposed strategy. After carefully checking the numerical procedure the authors concluded that the cause of this disagreement did not reside in the model itself, rather in the measured contact force signals fed to the model.

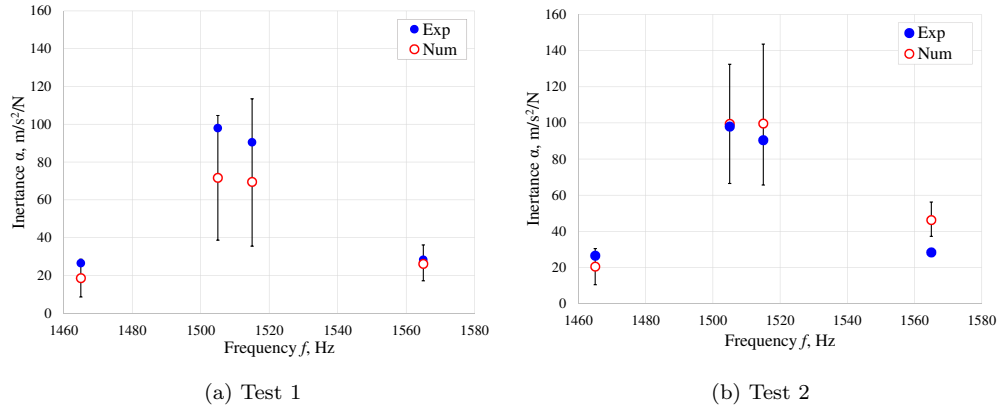


Figure 8: Comparison between the numerical and experimental blade response (loading conditions  $CF=26$  N and  $\mathbf{F_E}=1$  N). The error bars represent the variability of the numerical response resulting from feeding the model with measured contact forces considering their uncertainty.

To identify the source of errors two simpler experimental configurations

were investigated. In each test setup only one damper at a time was installed on one side of the blade, as depicted in Fig. 9. The numerical-experimental  
 240 comparison of both cases is shown in Fig. 10. Still a large discrepancy between the measured FRF and the numerical “prediction” can be observed in the first case when only the even side damper is active, Fig. 10a. Whereas, in the case in which the odd side damper is active, numerical results perfectly match with the experimentally measured amplitude response of the blade,  
 245 as shown in Fig. 10b.

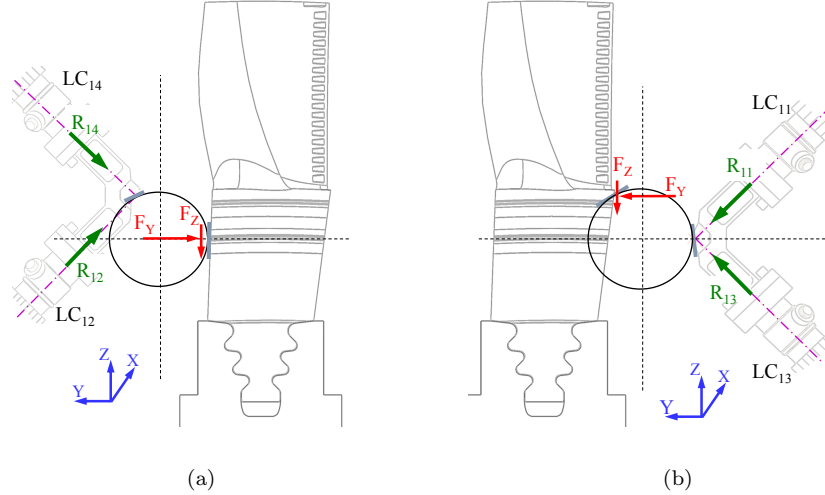


Figure 9: (a) Even side damper placed at its nominal position to measure contact forces.  
 (b) Odd side damper placed at its nominal position to measure contact forces

#### 4.2. Unsuccessful numerical-experimental comparison

The contact forces are composed of two parts: the “static” component that balance the simulated centrifugal force  $CF$  on the damper and the “dynamic” component (also referred to as “harmonic” component) deriving from  
 250 the blade movement. Figure 11 shows the contact forces on the even and odd

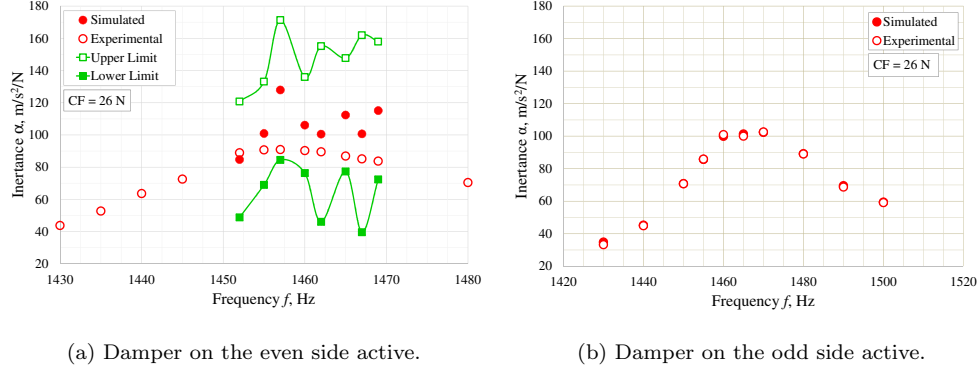


Figure 10: (a) Error sensitivity of blade response amplitude due to even side contact forces measurement at  $CF = 26$  N. (b) Numerical vs Experimental results comparison for damper forces measured on Odd side at  $CF = 26$  N

side platforms. In this figure, the contact forces are sketched at two distinct time points during blade movement - denoted by superscript prime and double prime - to emphasize the change, in magnitude and inclination, induced by blade dynamics. By carefully observing the contact forces on the even side platform, Fig. 11a, it is clear that the variation of force ranges between 1 to 2 N at the most. The magnitude of the harmonic variation of the force depends upon the contact angles and the platform kinematics (i.e. experimental set-up and blade mode shape). The level of uncertainty on the contact force,  $\approx 0.75$  N according to the sensitivity analysis performed in [30], is almost 50% of the force magnitude. This observation can easily explain the very large discrepancies between the numerical and experimental results: the platform blade has been loaded with a measured force whose measurement accuracy is of the same order of magnitude as the force itself.

A sensitivity analysis was carried out to further evaluate the effect of

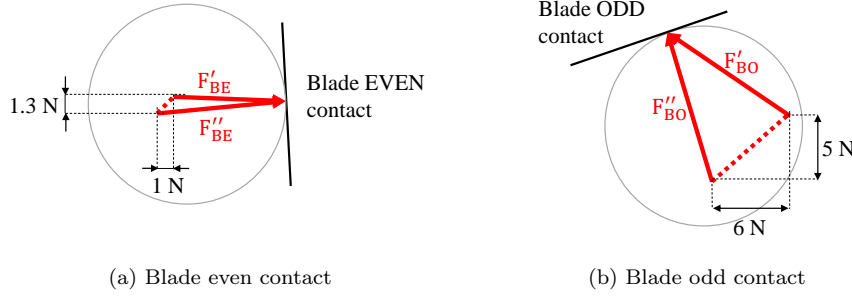


Figure 11: Measured contact force on the blade platform on the even and odd side,  $\mathbf{F}_{BE}$  and  $\mathbf{F}_{BO}$  respectively. The two forces on each side,  $\mathbf{F}'_{\mathbf{B}}$  and  $\mathbf{F}''_{\mathbf{B}}$ , are represented at two distinct time points of the same analysis. The picture emphasizes the variation of the contact forces caused by the blade movement.

the contact force measurement accuracy on the blade response. A sinusoidal perturbation was added to the contact force with a post-processing treatment of the measured signals. The amplitude of this perturbation was equal to the maximum level of uncertainty (0.75 N) with a phase shift that ranged from  
270 0 to 15 degrees with respect to the measured contact force. The upper and lower bound of the blade response produced by the perturbed contact force are shown in Fig. 10a. It is evident that even a seemingly small perturbation of this force can have a significant impact on the blade amplitude response.

#### 4.3. Successful numerical-experimental comparison

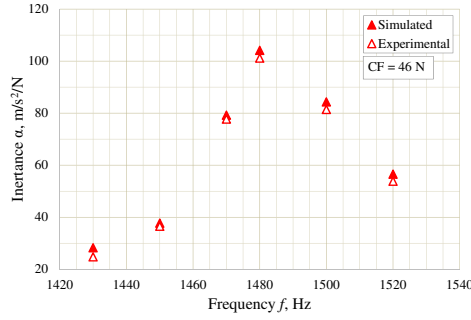
275 The second validation attempt was tested with only the even side damper activated, according to the configuration shown in Fig. 9b. The different contact angles of this configuration and the consequent platform kinematics, if compared with the results obtained with the activation of only the even side damper, produces

280

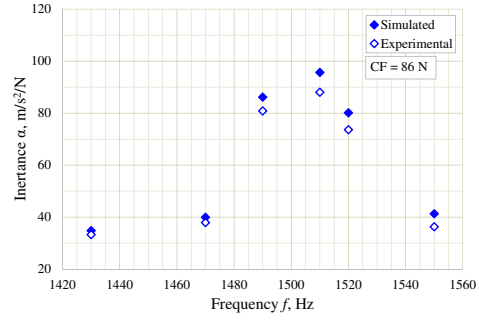
- higher harmonic variation of the measured contact forces that in this case range between 5 and 8 N, as shown in Fig. 11b;
- a stiffening effect, for which the peak in Fig.10b is now sharper and few Hz higher than that shown in Fig. 10a.

Furthermore, in this case, the uncertainty level guaranteed by the load cell measurement is adequate and reasonably smaller than the force signals themselves. As a result, the validation procedure summarized in Eq. 6 can be safely applied. Experiments were performed for three levels of load  $CF$  on the damper, namely 26, 46 and 86 N. Comparison between numerical and experimental results are shown in Fig. 10a ( $CF = 26$  N) and Fig. 12 ( $CF = 46$  and 86): numerical results match their experimental counterpart quite satisfactorily in all investigated cases.

290



(a) Case with centrifugal force  $CF = 46$  N.



(b) Case with centrifugal force  $CF = 86$  N.

Figure 12: Comparison of numerical and experimental frequency response amplitude for different loads  $CF$  on the damper.

## 5. Predicting influence of platform angles on the contact forces magnitude

Section 4 has shown that, depending on the damper position (i.e. the  
295 contact angles), the resulting amplitude of the harmonic component of the  
contact forces may change significantly. Attaining harmonic contact forces  
of adequate amplitude on the blade is of paramount importance, both in the  
laboratory environment and in real working conditions. An insufficient har-  
monic contact force amplitude influences the quality of the measurement in  
300 the lab as shown in Sect. 3, while it may impair the damping and stiffening  
effectiveness of the UPD as demonstrated in [39].

The purpose of this section is to provide the experimenter and blade/damper  
designer with a tool to predict the magnitude of the contact forces for differ-  
ent sets of platform angles.

### 305 5.1. The implicit stiffness concept

As shown in [40], the cylindrical damper analyzed in this paper never  
leaves the microslip condition. Therefore a conservative and representative  
modeling choice sees the damper in full stick (i.e. linked to the surrounding  
platforms by means of simple contact springs), as shown in Fig. 13a.

310 Since the damper is modeled as a rigid body and the position of the con-  
tact points is known (i.e. determined by the contact angles  $\theta_L$  and  $\theta_R$ ), it  
is convenient to substitute the presence of the damper with a set of equiv-  
alent springs, here termed implicit stiffness matrix  $\mathbf{K_I}$  and represented in  
Fig. 13b. This substitution willingly neglects the mass and inertia contribu-  
315 tion of the damper: this simplification is allowed since, as demonstrated in

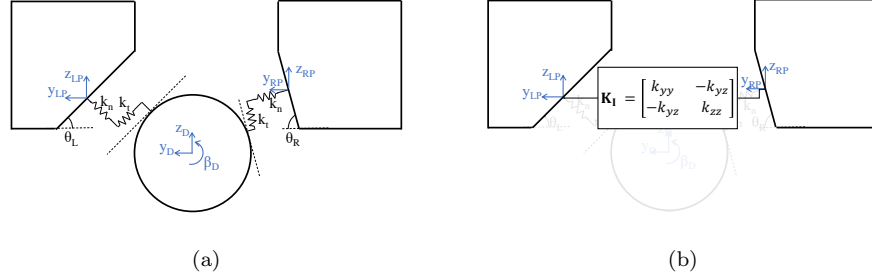


Figure 13: (a) 2D view of a damper between neighboring platforms in full stick condition. (b) Equivalent implicit stiffness concept.

[41], the damper inertial effects become significant only for frequencies  $>50$  kHz. In other words, the implicit stiffness  $\mathbf{K_I}$  takes into account the value and the position of the contact springs: the entries of matrix  $\mathbf{K_I}$  are linear combinations of the normal and tangential contact stiffness  $k_n$  and  $k_t$ , whose  
320 specific values have been determined according to [40]. The reader can refer to Appendix A for the complete derivation of  $\mathbf{K_I}$ .

## 5.2. A step-by-step procedure

This section aims at providing the reader with a series of instructions to predict the influence of the platform angles on the amplitude of the harmonic  
325 component of the contact forces. This task is of primary importance as it has been shown in Sect. 4 that the amplitude of the harmonic component of the contact forces can impair the model validation of the damper-blade system.

This procedure can be considered a standard sensitivity analysis. The input  
330 parameter space is composed by the two variables  $\theta_L$  and  $\theta_R$  which are explored in the  $[0 - 90]^\circ$  range. The "input" data of the sensitivity analysis is the FE model of the structure of interest. The following procedure, visual-



ized in Fig. 14, is repeated for all possible combinations of variables  $\theta_L$  and  $\theta_R$  explored in the range of interest.

- 335      3. The user adds the implicit stiffness contribution  $\mathbf{K}_I(\theta_L, \theta_R)$ , therefore matrix  $\mathbf{K}_R$  turns into matrix  $\mathbf{K}_{R,stick}$ . In the present case the user is trying to replicate the test condition from Fig.9, therefore  $\mathbf{K}_I$  is placed between contact nodes belonging to one of the platforms (either even or odd side) and the ground<sup>1</sup>.
- 340      4. Perform an eigenvalue analysis on matrices  $\mathbf{K}_{R,stick}$  and  $\mathbf{M}_R$  and isolate the mode of interest, here termed  $\phi_n$ .
5. The entries of mode  $\phi_n$  corresponding to the platform contact nodes DOFs represent the platform motion trajectory  $\phi_n(id_C)$ .
6. The normalized platform motion trajectory  $\frac{\phi_n(id_C)}{|\phi_n(id_C)|}$  multiplied by the  
345      implicit stiffness matrix  $\mathbf{K}_I$  yields the vector of normalized contact forces  $\mathbf{f} = (f_y, f_z)'$ .

The procedure is repeated for all  $(\theta_L, \theta_R)$  of interest. The  $y$  and  $z$  components of the target vector  $\mathbf{f}(\theta_L, \theta_R)$  can then be plotted as a function of the

---

<sup>1</sup>This procedure is taking advantage of two simplifications outlined below.

- (a) The ground platform is here not modeled since, as shown in [30], its stiffness is at least one order of magnitude larger than that of the blade and of the contact  $k_n$  and  $k_t$ .
- (b) In principle the blade platform geometry (i.e. inclination) should be updated to accommodate the different  $(\theta_L, \theta_R)$  combinations. However this minor geometrical change will not affect the subsequent eigenvalue analysis, therefore this step can be safely neglected.

two variables  $(\theta_L, \theta_R)$ . The results for a blade-single damper configuration  
 350 (similar to those shown in Fig. 9) can be found in Fig. 15. In detail, the  
 results related to the set-up which sees the damper on the left (even) side of  
 the blade can be found in Fig. 15a, those related to the damper on the right  
 (odd) side in Fig. 15b.

### 5.3. Results discussion

355 For each configuration, one point on the  $(\theta_L, \theta_R)$  plane corresponds to  
 the specific blade tested by the authors. This point has been highlighted  
 in Fig. 15. The comparison between the even and odd configuration fully  
 confirms the experimental results discussed in Fig. 11: the response surface  
 related to the even side configuration has a minimum in the area where the  
 360 experimental point lies. It is worth noticing that, had this tool been available  
 to the authors before the start of the experimental campaign, the even side  
 configuration would have been immediately discarded, thus saving time and  
 effort.

This comparison confirms the goodness of the implicit stiffness prediction  
 365 tool. The method can therefore be used to replicate a case of practical  
 interest, i.e. blades/dampers on a disk. In this case, the cyclic symmetry  
 framework can be used to test different engine order excitations [42]: the left  
 blade platform can be connected to the right one by  $K_I$  with a proper phase  
 shift (i.e. inter-blade phase angle).

## 370 6. Conclusions

This paper has presented a distinctive analysis procedure to investigate  
 the dynamic behavior of the blade with under-platform dampers. The con-

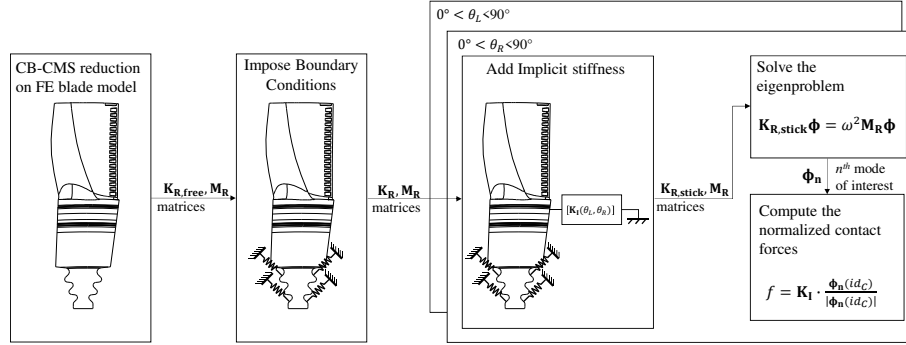


Figure 14: Graphical representation of the algorithm used to predict the normalized contact forces as a function of the blade platform angles.

tact forces between the damper-blade contact interfaces were the prime focus of the study. Experimental data were obtained by using a test rig which of-

375 fers the unique feature to measure the contact forces between the damper and the under-platform of the blade. In this test rig, two dampers were in contact with the respective platform of the blade. This feature gives the unprecedented opportunity to perform an experimental-numerical comparison which is independent of the chosen contact model. Knowledge of the contact

380 forces combined with the forced-response of the blade has allowed a deeper analysis of the dynamic behavior of the complete system. The blade was modeled with a commercial finite element code. In the next step, the mass and stiffness matrices of the blade were reduced, with a standard reduction order method, and extracted for further analysis to be performed with a in-

385 house code. The reduced model was constrained to simulate the attachment between the blade and the slot machined in the turbine blade clamp adapter on the test rig. The attachment was simulated with contact springs assuming that no sliding occurs between the mating surfaces. During the experimen-

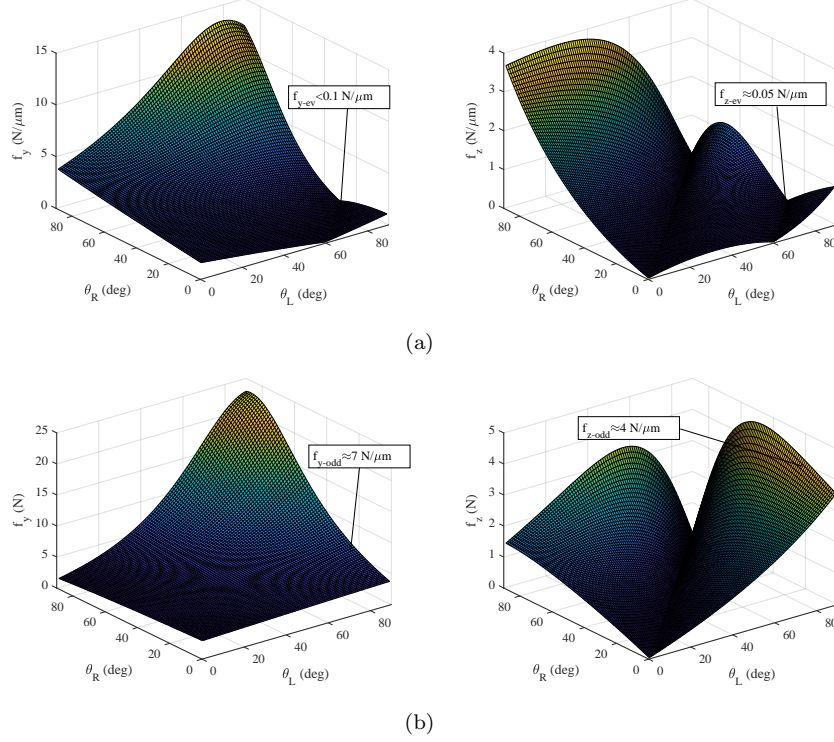


Figure 15:  $y$  and  $z$  components of the normalized contact force vector  $f$  when the damper is placed on the blade's (a) even and (b) odd side.

tal campaign contact forces at the blade-damper interface were measured  
 390 simultaneously with the forced-responses of the blade. These experimental  
 evidence were used to verify whether the measured contact forces applied to  
 the linear model of the blade yielded to a forced-response consistent with  
 the measured response. The results of the comparison were excellent on one  
 damper but unsatisfactory on the other one. To investigate this puzzling  
 395 behavior, a sensitivity analysis based on the concept of equivalent implicit  
 stiffness was performed on both dampers. This analysis showed that the  
 contact forces evaluated on the damper that exhibited poor matching with

the experimental results, were quite insensitive to the variation of damper geometry, namely the right and left contact angles. Moreover, these contact  
400 forces were very low and close to the measurement accuracy of the experimental system so that the determination of the value of these forces was an ill-conditioned problem. As a consequence, uncertainty in determining the contact forces value produces a large variation of the predicted force-response and then poor agreement with experimental results.

405 This work presents the validation of a contact models through experimental results under a different point of view. The main outcome is that when comparing the experimental results with a numerical simulation great attention must be paid to the source of experimental data. Some damper-underplatform configurations give contact forces that can be predicted with  
410 great uncertainty.

As underlined in the paper, in such conditions the computed forced-response of the blade is inaccurate, even if the measured contact forces are directly applied - during the simulation - to the contact nodes. The damper-underplatform geometry presented in this work is used in several friction  
415 damping systems, therefore the results presented in this work warning for all the designers and researches involved in a validation process. The proposed methodology to predict the amplitude of the contact forces starting from the platform angles constitutes one of the main contributions of this paper, as this methodology can be extended to the case of blades mounted on a disk  
420 in real working conditions.

## Appendix A. The implicit stiffness: derivation

With reference to Fig. 13a, let us consider the in-plane<sup>2</sup> equilibrium equations of a damper between a set of platforms with angles  $\theta_L$  and  $\theta_R$ .

$$\mathbf{M}_D \ddot{\mathbf{Q}}_D(t) = \mathbf{F}_{CD}(t) + \mathbf{F}_{ED} \quad (\text{A.1})$$

where  $\mathbf{Q}_D = (y_D, z_D, \beta_D)'$  is the vector of damper displacements,  $\mathbf{F}_{ED} = (0, CF, 0)'$  is the vector of external forces and  $\mathbf{F}_{CD}$  is the vector of contact forces transported at the damper center of mass. In case of full stick condition Eq. A.1 can be re-written as:

$$\mathbf{M}_D \ddot{\mathbf{Q}}_D(t) + \mathbf{K}_D \mathbf{Q}_D(t) = \mathbf{K}_P \mathbf{Q}_P(t) + \mathbf{F}_{ED} \quad (\text{A.2})$$

where  $\mathbf{Q}_P = (y_{LP}, z_{LP}, y_{RP}, z_{RP})'$  is the vector of platforms displacements (considered as an external information at this stage), and  $\mathbf{K}_D$  and  $\mathbf{K}_P$  are the contact stiffness matrices connected to damper and platforms respectively. The contact stiffness matrices can be expressed as:

$$\begin{aligned} \mathbf{K}_D &= \mathbf{T}' \mathbf{K}_{\text{local}} \mathbf{T} \\ \mathbf{K}_P &= \mathbf{T}' \mathbf{K}_{\text{local}} \mathbf{R} \end{aligned} \quad (\text{A.3})$$

where matrix  $\mathbf{K}_{\text{local}}$  is diagonal and function of the contact stiffness values  $\mathbf{K}_{\text{local}} = \text{diag}(k_t, k_n, k_t, k_n)^3$ . The reader will notice that the contact springs are oriented along the normal and tangential directions to each contact interface. For this reason, a local reference system has been defined

---

<sup>2</sup>The following derivation holds for in-plane motion for simplicity. However, a 3D version can be easily implemented.

<sup>3</sup>In case of 3D motion the matrix will become  $\mathbf{K}_{\text{local}} = \text{diag}(k_t, k_t, k_n, k_t, k_t, k_n)$ .

for each interface (left and right).  $\mathbf{T}$  is a transformation matrix of forces and displacements from the global (damper center of mass) to the local (i.e. damper contact points) reference system and viceversa. Similarly  $\mathbf{R}$  is a rotation matrix from global to local reference system, used for the platforms DOFs. Both matrices are a function of the platform angles  $\theta_L$  and  $\theta_R$ .

If variation of forces and displacements are considered, Eq. A.2 becomes:

$$\mathbf{K}_D \Delta \mathbf{Q}_D = \mathbf{K}_P \Delta \mathbf{Q}_P \quad (\text{A.4})$$

where the inertial terms can be neglected as demonstrated in [41] and  $\Delta \mathbf{F}_{ED} = \mathbf{0}$  since the centrifugal force is a constant term. The damper displacement variation  $\Delta \mathbf{Q}_D$  is expressed as:

$$\Delta \mathbf{Q}_D = \mathbf{K}_D^{-1} \mathbf{K}_P \Delta \mathbf{Q}_P \quad (\text{A.5})$$

Then the vector of contact forces in global coordinate system at the platform contact points can be expressed as:

$$\Delta \mathbf{F} = \mathbf{R}' \mathbf{K}_{\text{local}} (\mathbf{R} - \mathbf{T} \mathbf{K}_D^{-1} \mathbf{K}_P) \cdot \Delta \mathbf{Q}_P \quad (\text{A.6})$$

Where  $\Delta \mathbf{F} = (\Delta \mathbf{F}_{LP,y}, \Delta \mathbf{F}_{LP,z}, \Delta \mathbf{F}_{RP,y}, \Delta \mathbf{F}_{RP,z})'$  is the vector of contact forces on the two blade platforms. It is then possible to write:

$$\Delta \mathbf{F} = \mathbf{K}_I^* \Delta \mathbf{Q}_P \quad (\text{A.7})$$

where  $\mathbf{K}_I^*$  has the following structure:

$$\mathbf{K}_I^* = \begin{bmatrix} \mathbf{K}_I & -\mathbf{K}_I \\ -\mathbf{K}_I & \mathbf{K}_I \end{bmatrix} = \begin{bmatrix} k_{yy} & k_{yz} & -k_{yy} & -k_{yz} \\ k_{yz} & k_{zz} & -k_{yz} & -k_{zz} \\ -k_{yy} & -k_{yz} & k_{yy} & k_{yz} \\ -k_{yz} & -k_{zz} & k_{yz} & k_{zz} \end{bmatrix} \quad (\text{A.8})$$

The matrix  $\mathbf{K_I}$  is here termed implicit stiffness matrix and can be used to link a blade to a neighboring structure, be it an adjacent blade (real working conditions) or a ground platform (test rig condition).

## 425 References

- [1] J. H. Griffin, Friction damping of resonant stresses in gas turbine engine airfoils, *J. Eng. Power* 102 (2) (1980) 329–333. doi:10.1115/1.3230256.
- 430 [2] W. Sextro, K. Popp, I. Wolter, Improved reliability of bladed disks due to friction dampers, in: *ASME Turbo Expo: Power for Land, Sea, and Air*, Vol. 4: Manufacturing Materials and Metallurgy; Ceramics; Structures and Dynamics; Controls, Diagnostics and Instrumentation; Education, Orlando, Florida, USA, 1997, p. V004T14A035. doi:10.1115/97-GT-189.
- 435 [3] J. G. Malte Krack, *Harmonic Balance for Nonlinear Vibration Problems*, Springer-Verlag GmbH, 2019.  
URL [https://www.ebook.de/de/product/36171062/malte\\_krack\\_johann\\_gross\\_harmonic\\_balance\\_for\\_nonlinear\\_vibration\\_problems.html](https://www.ebook.de/de/product/36171062/malte_krack_johann_gross_harmonic_balance_for_nonlinear_vibration_problems.html)
- 440 [4] Y. Sun, J. Yuan, L. Pesaresi, E. Denimal, L. Salles, Parametric study and uncertainty quantification of the nonlinear modal properties of frictional dampers, *Journal of Vibration and Acoustics* 142 (5) (may 2020). doi:https://doi.org/10.1115/1.4046953.



- [5] B. D. Yang, C. H. Menq, Characterization of contact kinematics and application to the design of wedge dampers in turbomachinery blading: part 1—stick-slip contact kinematics, J. Eng. Gas Turbines Power 120 (2) (1998) 410–417. doi:10.1115/1.2818138.
- [6] B. D. Yang, C. H. Menq, Characterization of contact kinematics and application to the design of wedge dampers in turbomachinery blading: part 2—prediction of forced response and experimental verification, J. Eng. Gas Turbines Power 120 (2) (1998) 418–423. doi:10.1115/1.2818139.
- [7] G. Csaba, Modelling of a microslip friction damper subjected to translation and rotation, in: ASME 1999 International Gas Turbine and Aero-engine Congress and Exhibition, American Society of Mechanical Engineers, 1999, pp. V004T03A012–V004T03A012.
- [8] K. Y. Sanliturk, D. J. Ewins, A. B. Stanbridge, Underplatform dampers for turbine blades: theoretical modelling, analysis and comparison with experimental data, in: ASME 1999 international gas turbine and aero-engine congress and exhibition, American Society of Mechanical Engineers, 1999, pp. V004T03A037–V004T03A037.
- [9] L. Panning, W. Sextro, K. Popp, Optimization of interblade friction damper design, in: ASME Turbo Expo: Power for Land, Sea, and Air, Vol. 4: Manufacturing Materials and Metallurgy; Ceramics; Structures and Dynamics; Controls, Diagnostics and Instrumentation; Education, Munich, Germany, 2000, p. V004T03A068. doi:10.1115/2000-GT-0541.

- [10] E. P. Petrov, D. J. Ewins, Analytical formulation of friction interface elements of nonlinear multi-harmonic vibrations of bladed discs, in: ASME (Ed.), Turbo Expo: Power for Land, Sea, and Air, Vol. 4: Turbo Expo 2002, Parts A and B, Amsterdam, 2002, pp. 899–908. doi:10.1115/GT2002-30325.
- [11] S. Zucca, D. Botto, M. M. Gola, Range of variability in the dynamics of semi-cylindrical friction dampers for turbine blades, in: ASME Turbo Expo 2008: Power for Land, Sea, and Air, American Society of Mechanical Engineers, ASME, 2008, pp. 519–529. doi:10.1115/GT2008-51058.
- [12] L. Pesaresi, L. Salles, A. Jones, J. Green, C. Schwingshackl, Modelling the nonlinear behaviour of an underplatform damper test rig for turbine applications, Mech. Syst. Sig. Process. 85 (2017) 662–679. doi:10.1016/j.ymssp.2016.09.007.
- [13] S. Baek, B. Epureanu, Contact model identification for friction ring dampers in blisks with reduced order modeling, International Journal of Non-Linear Mechanics 120 (2020) 103374. doi:https://doi.org/10.1016/j.ijnonlinmec.2019.103374.
- [14] C. W. Schwingshackl, E. P. Petrov, D. J. Ewins, Effects of contact interface parameters on vibration of turbine bladed disks with underplatform dampers, J. Eng. Gas Turbines Power 134 (3) (2012) 032507. doi:10.1115/1.4004721.
- [15] C. Gastaldi, Modeling Friction for Turbomachinery Applications: Tun-

- 490 ing Techniques and Adequacy Assessment of Heuristic Contact Models,  
InTech, 2018. doi:10.5772/intechopen.72676.
- [16] M. Umer, D. Botto, Measurement of contact parameters on under-  
platform dampers coupled with blade dynamics, *Int. J. Mech. Sci.*  
(2019). doi:10.1016/j.ijmecsci.2019.06.010.
- 495 [17] I. A. Sever, E. P. Petrov, D. J. Ewins, Experimental and numerical in-  
vestigation of rotating bladed disk forced response using underplatform  
friction dampers, *ASME J. Eng. Gas Turbines Power* 130 (4) (2008)  
042503–11. doi:10.1115/1.2903845.
- [18] T. Berruti, A test rig for the investigation of the dynamic response of a  
500 bladed disk with underplatform dampers, *Mech. Res. Commun.* 37 (6)  
(2010) 581–583. doi:10.1016/j.mechrescom.2010.07.008.
- [19] A. Bessone, F. Toso, T. Berruti, Investigation on the dynamic response  
of blades with asymmetric under platform dampers, in: *ASME Turbo  
Expo: Power for Land, Sea, and Air*, Vol. 7B: Structures and Dy-  
namics, Montreal, Quebec, Canada, 2015, p. V07BT33A003. doi:  
505 10.1115/GT2015-42597.
- [20] C. W. Schwingshackl, E. P. Petrov, D. J. Ewins, Validation of test rig  
measurements and prediction tools for friction interface modelling, in:  
*ASME Turbo Expo: Power for Land, Sea, and Air*, Vol. 6, 2010. doi:  
510 10.1115/GT2010-23274.
- [21] D. Botto, M. Lavella, M. M. Gola, Measurement of contact parame-  
ters of flat on flat contact surfaces at high temperature, in: *Volume*

- 7: Structures and Dynamics, Parts A and B, ASME, 2012. doi:  
10.1115/GT2012-69677.
- 515 [22] D. Botto, M. Lavella, High temperature tribological study of cobalt-  
based coatings reinforced with different percentages of alumina, *Wear*  
318 (1-2) (2014) 89–97. doi:10.1016/j.wear.2014.06.024.
- [23] M. Lavella, D. Botto, M. M. Gola, Design of a high-precision, flat-on-  
flat fretting test apparatus with high temperature capability, *Wear* 302  
520 (2013) 1073–1081. doi:10.1016/j.wear.2013.01.066.
- [24] M. M. Gola, M. Braga dos Santos, T. Liu, Design of a new test rig to  
evaluate underplatform damper performance, in: ASME 2010 10th Bi-  
ennial Conference on Engineering Systems Design and Analysis, Vol. 5,  
2010, pp. 85–95. doi:10.1115/ESDA2010-24268.
- 525 [25] C. Gastaldi, M. M. Gola, A random sampling strategy for tuning contact  
parameters of underplatform dampers, in: Volume 7B: Structures and  
Dynamics, ASME International, 2015. doi:10.1115/GT2015-42834.
- [26] C. Gastaldi, M. M. Gola, Pre-optimization of asymmetrical under-  
platform dampers, *J. Eng. Gas Turbines Power* 139 (1) (2016) 1229.  
530 doi:10.1115/1.4034191.
- [27] D. Li, D. Botto, C. Xu, T. Liu, M. Gola, A micro-slip friction mod-  
eling approach and its application in underplatform damper kinemat-  
ics, *International Journal of Mechanical Sciences* 161-162 (2019) 105029.  
doi:10.1016/j.ijmecsci.2019.105029.

- 535 [28] D. Botto, M. Lavella, A numerical method to solve the normal and tangential contact problem of elastic bodies, *Wear* 330-331 (2015) 629–635. doi:10.1016/j.wear.2015.02.046.
- [29] D. Botto, M. Umer, C. Gastaldi, M. M. Gola, An experimental investigation of the dynamic of a blade with two under-platform dampers, in: Volume 7B: Structures and Dynamics, American Society of Mechanical  
540 Engineers, 2017. doi:10.1115/gt2017-64928.
- [30] D. Botto, M. Umer, A novel test rig to investigate under-platform damper dynamics, *Mech. Syst. Sig. Process.* 100 (2018) 344–359. doi:10.1016/j.ymssp.2017.07.046.
- 545 [31] C. Gastaldi, T. M. Berruti, M. M. Gola, A novel test rig for friction parameters measurement on underplatform dampers, *Int. J. Solids Struct.* 185-186 (2019) 170–181. doi:10.1016/j.ijsolstr.2019.08.030.
- [32] R. Craig, M. Bampton, Coupling of substructures for dynamic analyses, *AIAA journal* 6 (7) (1968) 1313–1319. doi:10.2514/3.4741.
- 550 [33] W. C. Hurty, Dynamic analysis of structural systems using component modes, *AIAA journal* 3 (4) (1965) 678–685.
- [34] J. Yuan, F. El-Haddad, L. Salles, C. Wong, Numerical assessment of reduced order modeling techniques for dynamic analysis of jointed structures with contact nonlinearities, *Journal of Engineering for Gas Turbines and Power* 141 (3) (nov 2018). doi:https://doi.org/10.1115/1.4041147.  
555

- [35] T. M. Cameron, J. H. Griffin, An alternating frequency/time domain method for calculating the steady-state response of nonlinear dynamic systems, *J. Appl. Mech.* 56 (1) (1989) 149–154.
- 560 [36] A. Cardona, T. Coune, A. Lerusse, M. Geradin, A multiharmonic method for non-linear vibration analysis, *Int. J. Numer. Methods Eng.* 37 (9) (1994) 1593–1608.
- [37] C. M. Furrone, S. Zucca, M. M. Gola, The effect of underplatform dampers on the forced response of bladed disks by a coupled static/dynamic harmonic balance method, *Int. J. Non Linear Mech.* 565 46 (2) (2011) 363–375. doi:10.1016/j.ijnonlinmec.2010.10.001.
- [38] M. Krack, L. Salles, F. Thouverez, Vibration prediction of bladed disks coupled by friction joints, *Arch. Comput. Methods Eng.* (jul 2016). doi:10.1007/s11831-016-9183-2.
- 570 [39] C. Gastaldi, M. M. Gola, Criteria for best performance of pre-optimized solid dampers, *J. Eng. Gas Turbines Power* 141 (4) (2018) 042502. doi:10.1115/1.4040820.
- [40] M. Umer, C. Gastaldi, D. Botto, The effect of friction damping on the dynamic response of vibrating structures: An insight into model validation, in: *Proceedings of ISMA 2018 - International Conference on Noise and Vibration Engineering and USD 2018 - International Conference on Uncertainty in Structural Dynamics*, 2018, pp. 1021–1035.
- 575 [41] C. Gastaldi, Vibration control and mitigation in turbomachinery, Ph.D.

thesis, Politecnico di Torino Italy (2017). doi:10.6092/polito/porto/2677053.

- [42] C. Gastaldi, T. M. Berruti, M. M. Gola, Best practices for underplatform damper designers, Proceedings of the Institution of Mechanical Engineers, Part C: Journal of Mechanical Engineering Science 232 (7) (2018) 1221–1235. doi:10.1177/0954406217753654.